

DISCOVERING HIDDEN FACTORS OF VARIATION IN DEEP NETWORKS

Brian Cheung^{*126}, Jesse A. Livezey^{*136}, Arjun K. Bansal⁶, & Bruno A. Olshausen¹⁴⁵

Redwood Center for Theoretical Neuroscience¹

Vision Science²

Department of Physics³

School of Optometry⁴

Helen Wills Neuroscience Institute⁵

University of California, Berkeley

Berkeley, CA 94720, USA

{bcheung, jesse.livezey, baolshausen}@berkeley.edu

Nervana Systems, Inc.⁶

San Diego, CA 92121, USA

arjun@nervanasys.com

* indicates equal contribution

ABSTRACT

We propose a method for learning latent representations of the factors of variation in data. By augmenting deep autoencoders with a supervised cost and an additional unsupervised cost, we create a semi-supervised model that can discover and explicitly represent factors of variation beyond those relevant for categorization. We use a novel unsupervised covariance penalty (XCov) to disentangle factors like handwriting style for digits and subject identity in faces. We demonstrate this on the MNIST handwritten digit database, the Toronto Faces Database (TFD) and the Multi-PIE dataset by generating manipulated instances of the data. Furthermore, we demonstrate these deep networks can extrapolate ‘hidden’ variation in the supervised signal using the Toronto Faces Database.

1 INTRODUCTION

One of the goals of representation learning is to find an efficient representation of input data that simplifies tasks such as object classification (Krizhevsky et al., 2012) or image restoration (Eigen et al., 2013). Supervised algorithms approach this problem by learning features which transform the data into a space where different classes are linearly separable. However this often comes at the cost of discarding other variations such as style or pose that may be important for more general tasks. On the other hand, unsupervised learning algorithms such as autoencoders seek efficient representations of the data such that the input can be fully reconstructed, implying that the latent representation preserves all factors of variation in the data. However, without some explicit means for factoring apart the different sources of variation the factors relevant for a specific task such as categorization will be entangled with other factors across the latent variables. Our goal in this work is to combine these two approaches in order to develop a model that preserves but also separates apart the different factors of variation in the data.

Previous approaches to separating factors of variation in data, such as content vs. style (Tenenbaum & Freeman, 2000) or form vs. motion (Grimes & Rao, 2005; Olshausen et al., 2007; Hinton et al., 2011; Memisevic & Hinton, 2010; Berkes et al., 2009; Cadieu & Olshausen, 2012), have relied upon a bilinear model architecture in which the units representing different factors are combined multiplicatively. This approach was also recently utilized to separate facial emotion vs. identity using higher-order restricted Boltzmann machines (Reed et al., 2014). One downside of bilinear approaches in general is that they require learning a weight tensor corresponding to all three-way

multiplicative combinations of units. Oftentimes this is made more tractable by approximating the full tensor in terms of a sum of low-rank tensors, which reduces the number of weights to be learned. Despite the impressive results achieved with this approach, the question nevertheless remains as to whether there is a more straightforward way to separate factors of variation using standard nonlinearities in feedforward neural networks. Earlier work by Salakhutdinov & Hinton (2007) demonstrated class-irrelevant aspects in MNIST (style) can be learned by including additional unsupervised units alongside supervised ones in an autoencoder. However, their model does not disentangle class-irrelevant factors from class-relevant ones. More recently, Kingma et al. (2014) utilized a variational autoencoder in a semi-supervised learning paradigm which is capable of separating content and style in data. It is this work which is the inspiration for the model presented here.

Autoencoder models have been shown to be useful for a variety of machine learning tasks (Rifai et al., 2011; Vincent et al., 2010; Le, 2013). The basic autoencoder architecture can be separated into an encoding stage and a decoding stage. During training, the two stages are jointly optimized to reconstruct the input data from the output of the decoder. Bengio et al. (2007) showed that greedy layerwise pre-training can speed up the convergence and improve generalization capabilities of deep networks. After pre-training, the decoder is discarded and the network is fine-tuned on labeled data. Such autoencoder models are now a standard framework in many machine learning pipelines, as they are easily trained by back propagation as compared to probabilistic generative models that require expensive sampling or other approximate methods to fit to the data.

In this work, we propose using both the encoding and decoding stages of the autoencoder to learn high-level representations of the factors of variation contained in the data. The high-level representation (or middle layer) is divided into two sets of variables. The first set (observed variables) is used in a discriminative task and during reconstruction. The second set (latent variables) is used only for reconstruction. For TFD, we find that the observed variables can extrapolate beyond values seen in training and represent ‘opposite’ expressions. In addition to the typical reconstruction cost, we add two additional costs to the network. The first is a discriminative cost on the observed variables such as cross-entropy. The second is a novel cross-covariance penalty (XCov) between the observed and latent variables across a batch of data. This penalty prevents latent variables from encoding input variations due to class label. In this way, the variables which represent class assignment are separated from those which are encoding other factors of variations in the data. The model is trained with backpropagation using the common MLP layer types (in this case, RELU and linear), and can use a combination of labeled, partially labeled, and unlabeled data.

2 MODEL

Given a data sample $x \in \mathbb{R}^D$ and its corresponding class label $y \in \{1, \dots, L\}$ for a dataset \mathcal{D} , our model can be decomposed into an encoding and a decoding stage.

2.1 ENCODING

The encoder $F(x; \theta)$ is comprised of two functions with parameters $\theta = \{\theta_h, \theta_z, \theta_y\}$.

$$\begin{aligned}\hat{y} &= q(x; \theta_y, \theta_h) \\ z &= r(x; \theta_z, \theta_h) \\ \{\hat{y}, z\} &= F(x; \theta) \equiv \{q(x), r(x)\}\end{aligned}\tag{1}$$

As shown in Figure 1, the encoder first transforms the input x into a tuple of variables: $\{\hat{y}, z\}$. The label prediction \hat{y} has an encoding process $\hat{y} = q(x)$ which is functionally equivalent to a supervised feedforward network. z is an additional latent representation of x which is similar to the representation generated at any sufficiently deep layer during the feedforward process of an autoencoder. To keep our formulation simple, z is at the same depth as \hat{y} .

2.2 DECODING

The decoder $G(\hat{y}, z; \phi)$ transforms the tuple provided by the encoder into a reconstruction \hat{x} . Combining the encoding and decoding steps defines the forward process of our model:

$$\hat{x} = G(y, z; \phi) = G(F(x; \theta); \phi). \quad (2)$$

The decoder must create a reconstruction \hat{x} which is as close to x as possible given the feature representation \hat{y} and z . The supervised term \hat{y} often represents a lossy transformation of the input x such as the class label. In order to properly reconstruct x , the latent variable z must account for the remaining variation of x . For example, the class label ‘5’ provided by y would not be sufficient information for the decoder to properly reconstruct the image of a particular digit ‘5’. In this scenario, z would encode properties of the digit such as style, slant, width, etc. to provide the decoder sufficient information to reconstruct the original image.

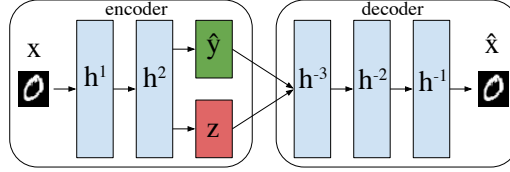


Figure 1: The encoder and decoder are combined and jointly trained to reconstruct the inputs and predict the observed variables \hat{y} .

2.3 LEARNING

With the forward process of the network defined, the objective function to train the network can be described:

$$\hat{\theta}, \hat{\phi} = \arg \min_{\theta, \phi} \sum_{\{x, y\} \in \mathcal{D}} \alpha U(x, \hat{x}) + \beta S(y, \hat{y}) + \gamma C(\hat{y}, z). \quad (3)$$

$U(x, \hat{x})$ is a reconstruction cost, $S(y, \hat{y})$ is a supervised cost of the encoder, and $C(\hat{y}, z)$ is the XCov cost which disentangles the observed and latent variables of the encoder.

This objective function naturally fits a semi-supervised learning framework. For unlabeled data, the multiplier β for the supervised cost S is simply set to zero. In general, the choice of α , β , and γ will depend on the intended task. Larger α will lead to better generative performance, β to classification performance, and γ to manipulation/transformation performance. When the objective, encoding, and decoding functions are differentiable, this model can be trained with stochastic gradient descent via backpropagation.

While there are many potential choices for the reconstruction cost depending on the distribution of data vector x , for our experiments we use mean-squared-error for all datasets which is defined as:

$$U(x, \hat{x}) = ||x - \hat{x}||^2. \quad (4)$$

$$S(y, \hat{y}) = \sum_{y_i} y_i \log(\hat{y}_i) \quad (5)$$

For the observed variables, the form of the cost function depends on the type of variables (categorical, binary, continuous). For our experiments, we had one or more categorical latent variables so we parametrized them as one-hot vectors and computed \hat{y} using a softmax activation with cross-entropy as the cost.

The XCov penalty to disentangle \hat{y} and z is simply a sum-squared cross-covariance penalty between the activations across samples in a batch of size N with formula and gradient defined as:

$$C(\hat{y}, z) = \frac{1}{2} \sum_{ij} [\frac{1}{N} \sum_n (\hat{y}_i^n - \bar{\hat{y}}_i)(z_j^n - \bar{z}_j)]^2 \quad (6)$$

$$\frac{\partial C(\hat{y}, z)}{\partial \hat{y}_a^m} = \sum_j [\frac{1}{N} \sum_n (\hat{y}_a^n - \bar{\hat{y}}_a)(\hat{z}_j^n - \bar{\hat{z}}_j)] [\frac{1}{N} (\hat{z}_j^m - \bar{\hat{z}}_j)] \quad (7)$$

$$\frac{\partial C(\hat{y}, z)}{\partial \hat{z}_b^m} = \sum_i [\frac{1}{N} \sum_n (\hat{y}_i^n - \bar{\hat{y}}_i)(\hat{z}_b^n - \bar{\hat{z}}_b)] [\frac{1}{N} (\hat{y}_i^m - \bar{\hat{y}}_i)] \quad (8)$$

where $\bar{\hat{y}}_i$ and $\bar{\hat{z}}_j$ denote means over examples, superscripts index examples, and subscripts index features. Unlike $U(x, \hat{x})$ and $S(y, \hat{y})$ in the objective, $C(\hat{y}, z)$ is a cost computed over a batch of datapoints. It is possible to approximate this quantity with a moving average during training but we have found that this cost has been robust to small batch sizes and have not found any issues when training with mini-batches of $N = 50$.

This penalty will only truly factorize $P(\hat{y}, z|x)dx$ into $P(\hat{y}|x)P(z|x)dx$ when $P(\hat{y}, z|x)dx$ is normally distributed. Despite this fact, we have found this penalty to work well regardless of the form of activation function (i.e. softmax, tanh, linear). Rifai et al. (2012) proposed a similar penalty in Contractive Discriminant Analysis method which penalized the cross-derivatives between sets of observed and latent variables with respect to the input.

3 EXPERIMENTAL RESULTS

We evaluate our model on three datasets of increasing complexity. The network is trained using AdaDelta (Zeiler, 2012) with gradients from standard backpropagation. Models were implemented in a modified version of Pylearn2 (Goodfellow et al., 2013a) using deconvolution and likelihood estimation code from Goodfellow et al. (2014).

3.1 MNIST HANDWRITTEN DIGITS DATABASE

The MNIST handwritten digits database (LeCun & Cortes, 1998) consists of 60,000 training and 10,000 test images of handwritten digits 0-9 of size 28x28. Following previous work (Goodfellow et al., 2013b), we split the training set into 50,000 samples for training and 10,000 samples as a validation set for model selection.

3.2 TORONTO FACES DATABASE

The Toronto Faces Database (Susskind et al., 2010) consists of 102,236 grayscale face images of size 48x48. Of these, 4,178 are labeled with 1 of 7 different expressions (anger, disgust, fear, happy, sad, surprise, and neutral). Examples are shown in Figure 2. The dataset also contains 3,784 identity labels which were not used in this paper. The dataset has 5 folds of training, validation and test examples.



Figure 2: Example TFD images from the test set showing 7 expressions with random identity.

3.3 MULTI-PIE DATASET

The Multi-PIE datasets (Gross et al., 2010) consists of 754,200 high-resolution color images of 337 subjects. Each subject was recorded under 15 camera poses: 13 spaced at 15 degree intervals at head height, and 2 positioned above the subject. For each of these cameras, subjects were imaged under 19 illumination conditions and a variety of facial expressions. We discarded images from the two overhead cameras due to inconsistencies found in the image orientation for those two cameras. Camera pose and illumination data was retained as supervised labels.

Only a small subset of the images possess facial keypoint information for each camera pose. To perform a weak registration to approximately localize the face region, we compute the maximum bounding box created by all available facial keypoint coordinates for a given camera pose. The bounding box is applied to all images for that camera pose. We then resized the cropped images to 48x48 pixels and convert to grayscale. We divide the dataset into 528,060 training, 65,000 validation and 60,580 test examples. Splits were determined by subject id. Therefore, the test set consists of subject identities never seen by our model. Example images from our test set are shown in Figure 3.



Figure 3: Example Multi-PIE images from the test set showing 3 of 19 camera poses with variable lighting and identity. Since not all images had keypoints tagged, there is some variability in face location.

The Multi-PIE dataset contains significantly more factors of variation than MNIST or TFD. Comparing example images from TFD in Figure 2 and Multi-PIE in Figure 3, it is clear that the Multi-PIE images are substantially more complex. The weak registration causes variation in head position and scale. While this could be alleviated with facial registration software, we forgo this preprocessing to demonstrate the robustness of our method.

3.4 EXPLORING DEEP SPACE

We begin our analysis using the MNIST dataset. After training the MNIST model described in Table 1, the function of hidden units in different layers can be explored. As shown in Figure 4, the latent variables z take on an approximate Normal distribution with mean zero and standard deviation ≈ 35 . We can generate digits from this approximate distribution and explore this smooth 2D latent space using the generative decoding network.

Table 1: Network Architectures (Softmax (SM), Rectified Linear (ReLU))

MNIST	TFD	ConvDeconvMultiPIE
500 ReLU	2000 ReLU	20x20x32 ConvReLU
500 ReLU	2000 ReLU	2000 ReLU
10 SM, 2 Linear	7 SM, 793 Linear	2000 ReLU
500 ReLU	2000 ReLU	13 SM, 19 SM, 793 Linear
500 ReLU	2000 ReLU	2000 ReLU
784 Linear	2304 Linear	2000 ReLU
		2000 ReLU
		2000 ReLU
		48x48x1 Deconv

3.4.1 LATENT VARIABLES

To visualize the transformations that the latent variables are learning, the decoder can be used to create images with different values for z . We select latent variable values by setting the z s to a linear range with y set up one-hot vectors as seen in Figure 4. At the center of z -space, (0,0), we find the canonical MNIST digits. Moving further from the center, the digits become more stylized and also less probable.

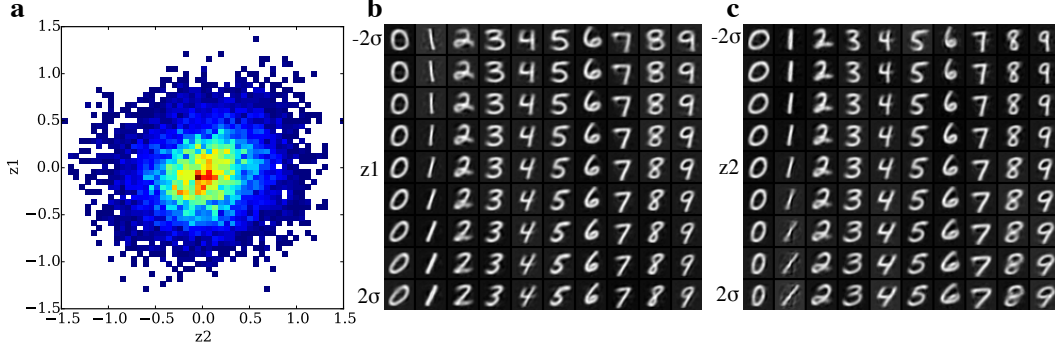


Figure 4: **a:** Histogram of test set z variables. **b:** Generated MNIST digits formed by setting z_2 to zero and varying z_1 . **c:** Generated MNIST digits formed by setting z_1 to zero and varying z_2 . σ was calculated from the variation on the test set.

3.4.2 MOVING FROM LATENT SPACE TO IMAGE SPACE

After the observed and latent variables, there are two more layers of activations before the output of the model into image space. To visualize the function of these layers, we compute the Jacobian of the output image, \hat{x} , with respect to the activation of hidden units, h^k , in a particular layer,

$$\Delta \hat{x}_i^k = \frac{\partial \hat{x}_i}{\partial h_j^k} \Delta h_j. \quad (9)$$

Here, i is the index of a pixel in the output of the network, j is the index of a hidden unit, and k is the layer number. We remove hidden units with zero activation from the Jacobian since their derivatives are not meaningful. A summary of the results are plotted in Figure 5.

For the Jacobian with respect to the z units, we plot the result in image space. As expected, the Jacobian with respect to the z units locally mirror the transformations seen in Figure 4.

Inspired by Rifai et al. (2011), for the next two layers, we plot the singular value spectrum. For h^{-3} , the spectrum is peaked and thus there are a small number of directions with large effect on the image output, so we plot singular vectors with largest singular value. For all digits besides “1”, the first component seems to create a template digit and the other components make small style adjustments. For h^{-2} , the spectrum is more degenerate, so we choose a random set of columns from the Jacobian to plot which will better represent the layer’s function. We notice that for each layer moving from the encoder to the output, their contributions become more localized.

3.5 GENERATING EXPRESSION TRANSFORMATIONS

We demonstrate semi-supervised capabilities of our model on the TFD which contains substantially more complex images than MNIST and has far fewer labeled examples. We are able to change the expression while preserving identity of faces never before seen by the model. We first initialize $\{\hat{y}, z\}$ with an example from the test set. We then discard \hat{y} and fill it in with an expression label and retain z . Figure 6 shows the results of this process. Expressions can be changed while leaving other facial characteristics largely intact. This is not possible when the XCov cost is removed, because the expression information is distributed across all 793 z variables in addition to the 7 y variables. Modifications to y do significantly impact the representation provided to the decoder.

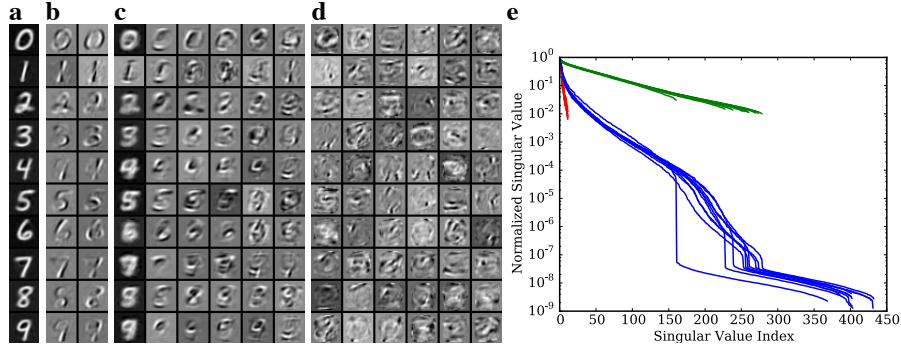


Figure 5: **a**: Jacobians were taken at activation values that lead to these images. z was set to zero for each digit class. **b**: Gradients of the decoder output with respect to z . **c**: Singular vectors from the Jacobian from the activations of the first layer after $\{y, z\}$. **d**: Column vectors from the Jacobian from the the activations of the second layer after $\{y, z\}$. Note that units in the columns for **d** are not necessarily the same unit. **e**: Plots of the normalized singular values for *red*: the Jacobians with respect to $\{y, z\}$, *blue*: the Jacobians with respect to the activations of the first layer after $\{y, z\}$ (h^{-3} in Fig. 1), and *green*: the Jacobians with respect to the activations of the second layer after $\{y, z\}$ (h^{-2} in Fig. 1).

3.5.1 EXTRAPOLATING OBSERVED VARIABLES

Additionally, y can be set to values well beyond those that the encoder could output with a softmax activation during training. We vary the expression variable given to the decoder from 5 to -5. This results in greatly exaggerated expressions when set to extreme positive values as seen in Figure 7. Remarkably, setting the variables to extreme negative values results in ‘negative’ facial expressions being displayed. These negative facial expressions are abstract opposites of their positive counterparts. When the eyes are open in one extreme, they are closed in the opposite extreme. This is consistent regardless of the expression and holds true for other abstract facial features such as open/closed mouth and smiling/frowning face. We consider these negative facial expressions extrapolations because the decoder never receives negative values for the observed variables during training. The model has learned a meaningful extrapolation of facial structure not explicitly present in the labeled data.

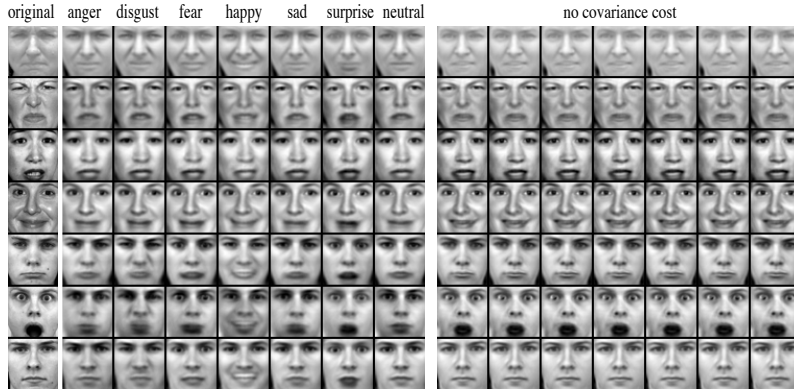


Figure 6: Left column: Samples from the test set displaying each of the 7 expressions. The expression-labeled columns are generated by keeping the latent variables z constant and changing y (expression). The rightmost set of faces are from a model with no covariance cost and showcase the importance of the cost in disentangling expression from the latent z variables.



Figure 7: For each column, y is set to a one-hot vector and scaled from 5 to -5 from top to bottom, well outside of the natural range of $[0,1]$. ‘Opposite’ expressions and more extreme expressions can be made.

3.6 MANIPULATING MULTIPLE FACTORS OF VARIATION

For Multi-PIE, we use two sets of observed factors (camera pose and illumination) to train our model. As shown in Table 1, we have two softmax layers at the end of the encoder. The first encodes the camera pose of the input image and the second the illumination condition. Due to the increased complexity of this dataset, we made this network substantially deeper (9 layers) than the previous models. It was possible to train this autoencoder without pre-training because of the additional gradient information injected by the supervised and covariance cost at the end of the encoder similar to Szegedy et al. (2014).

In Figure 8, we show the images generated by the decoder while iterating through each camera pose. The network was tied to the illumination and latent variables of images from the test set. Although blurry, the generated images preserve the subject’s illumination and identity (i.e. shirt color, hair style, skin tone) as the camera pose changes. In Figure 9, we instead fix the camera position and iterate through different illumination conditions.



Figure 8: Left column: Samples from test set with initial camera pose. The faces on the right were generated by changing the corresponding camera pose.

4 CONCLUSIONS

With the addition of a supervised cost and an unsupervised cross-covariance penalty, our model learns to disentangle various transformations using standard feedforward neural network components. We show the model can make use of labeled and unlabeled data simultaneously. Furthermore, the decoder of our model implicitly learns to generate novel manipulations of images on multiple sets of transformation variables. We show deep feedforward networks are capable of learning higher-order factors of variation beyond the observed labels without the need to explicitly define these higher-order interactions. Finally, we demonstrate the ability of these deep networks to extrapolate intrinsic variation present in the supervised signal.



Figure 9: Left column: Samples from test set. Illumination transformations are shown to the right. Ground truth lighting for the first face in each block is in the first row.

Table 2: MNIST Classification Performance

Model	Classification Accuracy	Model Selection Criterion
MNIST	98.35	Reconstruction: $\alpha = 1, \beta = 10, \gamma = 10$
ConvMNIST	98.71	Reconstruction: $\alpha = 1, \beta = 10, \gamma = 10$
MaxoutMNIST + dropout	99.01	Accuracy: $\alpha = 1, \beta = 100, \gamma = 10$
Maxout + dropout Goodfellow et al. (2013b)	99.06	Accuracy

ACKNOWLEDGMENTS

We are grateful for the helpful comments from reviewers. We would like to acknowledge everyone at the Redwood Center and beyond for their helpful discussion and comments. We thank Nervana Systems for supporting Brian Cheung during the summer when this project originated and for their continued collaboration. We gratefully acknowledge the support of NVIDIA Corporation with the donation of the Tesla K40 GPUs used for this research. Bruno Olshausen was supported by NSF grant IIS-1111765.

APPENDIX

CLASSIFICATION PERFORMANCE

Tables 2 and 3 show classification results for MNIST and TFD networks described in Table 4. With this model, it is possible to trade-off classification accuracy for reconstruction accuracy. Our methods are amenable to different nonlinearities such as Maxout (Goodfellow et al., 2013b) and different training algorithms such as SGD with momentum, SFO (Sohl-Dickstein et al., 2014), or Dropout (Srivastava et al., 2014). Performance of a fully connected maxout network used for the encoder similar to Goodfellow et al. (2013b) is also shown. Note that some models were selected based on classification accuracy rather than reconstruction accuracy.

Table 3: TFD Classification Performance

Model	Classification Accuracy	Model Selection Criterion
TFD	69.4	Reconstruction: $\alpha = 1, \beta = 10, \gamma = 1000$ (Fold 0)
ConvTFD	84.0	Accuracy: $\alpha = 1, \beta = 10, \gamma = 1000$ (Fold 0)
disBM Reed et al. (2014)	85.4	Accuracy
CCNET+CDA+SVM Rifai et al. (2012)	85.0	Accuracy (Fold 0)

Table 4: Network Architectures (Softmax (SM), Rectified Linear (ReLU))

ConvMNIST	MaxoutMNIST	ConvTFD
12x12x32 ConvReLU	240-5 Maxout	22x22x16 ConvReLU
500 ReLU	240-5 Maxout	2000 ReLU
10 SM, 2 Linear	10 SM, 2 Linear	7 SM, 793 Linear
500 ReLU	240-5 Maxout	2000 ReLU
500 ReLU	240-5 Maxout	2000 ReLU
784 Linear	784 Linear	2304 Linear

GENERATIVE PERFORMANCE

Table 5 shows Parzen-window based likelihood estimates from our models introduced in Breuleux et al. (2011). We use the code and results from Goodfellow et al. (2014). For our model, we first generate ys and zs from encoded training data. Then we fit a {Categorical, Normal} model to these latent variables and generate samples from this distribution and pass them into the decoder. We fit a Parzen-window model to these samples and evaluate the likelihood of the test set under this model. Cross validation of σ was done in the same way as Goodfellow et al. (2014). We do not report state-of-the-art results, but our results are competitive with many of the previous methods.

We also estimate an empirical upper bound by fitting the Parzen-window model on actual training examples and evaluating the likelihood of the test set.

It is important to note that the choice of a Normal distribution for zs is empirically and not theoretically motivated. We also artificially restricted the total latent space to 12 dimensions for the MNIST model to allow visualization.

REFERENCES

- Bengio, Yoshua, Lamblin, Pascal, Popovici, Dan, and Larochelle, Hugo. Greedy layer-wise training of deep networks. *Advances in neural information processing systems*, 19:153, 2007.
- Bengio, Yoshua, Mesnil, Gregoire, Dauphin, Yann, and Rifai, Salah. Better mixing via deep representations. In *Proceedings of The 30th International Conference on Machine Learning*, pp. 552–560, 2013.
- Bengio, Yoshua, Laufer, Eric, Alain, Guillaume, and Yosinski, Jason. Deep generative stochastic networks trainable by backprop. In *Proceedings of the 31st International Conference on Machine Learning (ICML-14)*, pp. 226–234, 2014.
- Berkes, Pietro, Turner, Richard E, and Sahani, Maneesh. A structured model of video reproduces primary visual cortical organisation. *PLoS computational biology*, 5(9):e1000495, 2009.
- Breuleux, Olivier, Bengio, Yoshua, and Vincent, Pascal. Quickly generating representative samples from an rbm-derived process. *Neural Computation*, 23(8):2058–2073, 2011.

Table 5: Generative Performance

Model	MNIST	TFD
Table 1 Models	138 ± 1.6	1913 ± 22
DBN Bengio et al. (2013)	138 ± 2	1909 ± 66
Stacked CAE Bengio et al. (2013)	121 ± 1.6	2110 ± 50
Deep GSN Bengio et al. (2014)	214 ± 1.1	1890 ± 29
Adversarial nets Goodfellow et al. (2014)	225 ± 2	2057 ± 26
Empirical Bound	241 ± 2.1	2129 ± 21

Cadieu, Charles F and Olshausen, Bruno A. Learning intermediate-level representations of form and motion from natural movies. *Neural computation*, 24(4):827–866, 2012.

Eigen, David, Krishnan, Dilip, and Fergus, Rob. Restoring an image taken through a window covered with dirt or rain. In *Computer Vision (ICCV), 2013 IEEE International Conference on*, pp. 633–640. IEEE, 2013.

Goodfellow, Ian, Pouget-Abadie, Jean, Mirza, Mehdi, Xu, Bing, Warde-Farley, David, Ozair, Sherjil, Courville, Aaron, and Bengio, Yoshua. Generative adversarial nets. In *Advances in Neural Information Processing Systems*, pp. 2672–2680, 2014.

Goodfellow, Ian J, Warde-Farley, David, Lamblin, Pascal, Dumoulin, Vincent, Mirza, Mehdi, Pascanu, Razvan, Bergstra, James, Bastien, Frédéric, and Bengio, Yoshua. Pylearn2: a machine learning research library. *arXiv preprint arXiv:1308.4214*, 2013a.

Goodfellow, Ian J, Warde-farley, David, Mirza, Mehdi, Courville, Aaron, and Bengio, Yoshua. Max-out networks. In *Proceedings of the 30th International Conference on Machine Learning*, pp. 1319–1327. ACM, 2013b.

Grimes, David B and Rao, Rajesh PN. Bilinear sparse coding for invariant vision. *Neural computation*, 17(1):47–73, 2005.

Gross, Ralph, Matthews, Iain, Cohn, Jeffrey, Kanade, Takeo, and Baker, Simon. Multi-pie. *Image and Vision Computing*, 28(5):807–813, 2010.

Hinton, Geoffrey E, Krizhevsky, Alex, and Wang, Sida D. Transforming auto-encoders. In *Artificial Neural Networks and Machine Learning–ICANN 2011*, pp. 44–51. Springer, 2011.

Kingma, Diederik P, Mohamed, Shakir, Rezende, Danilo Jimenez, and Welling, Max. Semi-supervised learning with deep generative models. In *Advances in Neural Information Processing Systems*, pp. 3581–3589, 2014.

Krizhevsky, Alex, Sutskever, Ilya, and Hinton, Geoffrey E. Imagenet classification with deep convolutional neural networks. In *Advances in neural information processing systems*, pp. 1097–1105, 2012.

Le, Quoc V. Building high-level features using large scale unsupervised learning. In *Acoustics, Speech and Signal Processing (ICASSP), 2013 IEEE International Conference on*, pp. 8595–8598. IEEE, 2013.

LeCun, Yann and Cortes, Corinna. The mnist database of handwritten digits, 1998.

Memisevic, Roland and Hinton, Geoffrey E. Learning to represent spatial transformations with factored higher-order boltzmann machines. *Neural Computation*, 22(6):1473–1492, 2010.

Olshausen, Bruno A, Cadieu, Charles, Culpepper, Jack, and Warland, David K. Bilinear models of natural images. In *Electronic Imaging 2007*, pp. 649206–649206. International Society for Optics and Photonics, 2007.

- Reed, Scott, Sohn, Kihyuk, Zhang, Yuting, and Lee, Honglak. Learning to disentangle factors of variation with manifold interaction. In *Proceedings of The 31st International Conference on Machine Learning*, pp. 1431-1439. ACM, 2014.
- Rifai, Salah, Vincent, Pascal, Muller, Xavier, Glorot, Xavier, and Bengio, Yoshua. Contractive auto-encoders: Explicit invariance during feature extraction. In *Proceedings of the 28th International Conference on Machine Learning (ICML-11)*, pp. 833-840, 2011.
- Rifai, Salah, Bengio, Yoshua, Courville, Aaron, Vincent, Pascal, and Mirza, Mehdi. Disentangling factors of variation for facial expression recognition. In *Computer Vision-ECCV 2012*, pp. 808-822. Springer, 2012.
- Salakhutdinov, Ruslan and Hinton, Geoffrey E. Learning a nonlinear embedding by preserving class neighbourhood structure. In *International Conference on Artificial Intelligence and Statistics*, pp. 412-419, 2007.
- Sohl-Dickstein, Jascha, Poole, Ben, and Ganguli, Surya. Fast large-scale optimization by unifying stochastic gradient and quasi-newton methods. In *Proceedings of the 31st International Conference on Machine Learning (ICML-14)*, pp. 604-612, 2014.
- Srivastava, Nitish, Hinton, Geoffrey, Krizhevsky, Alex, Sutskever, Ilya, and Salakhutdinov, Ruslan. Dropout: A simple way to prevent neural networks from overfitting. *The Journal of Machine Learning Research*, 15(1):1929-1958, 2014.
- Susskind, J., Anderson, A., and Hinton, G. E. The toronto face database. Technical report, University of Toronto, 2010.
- Szegedy, Christian, Liu, Wei, Jia, Yangqing, Sermanet, Pierre, Reed, Scott, Anguelov, Dragomir, Erhan, Dumitru, Vanhoucke, Vincent, and Rabinovich, Andrew. Going deeper with convolutions. *arXiv preprint arXiv:1409.4842*, 2014.
- Tenenbaum, Joshua B and Freeman, William T. Separating style and content with bilinear models. *Neural computation*, 12(6):1247-1283, 2000.
- Vincent, Pascal, Larochelle, Hugo, Lajoie, Isabelle, Bengio, Yoshua, and Manzagol, Pierre-Antoine. Stacked denoising autoencoders: Learning useful representations in a deep network with a local denoising criterion. *The Journal of Machine Learning Research*, 11:3371-3408, 2010.
- Zeiler, Matthew D. Adadelta: An adaptive learning rate method. *arXiv preprint arXiv:1212.5701*, 2012.